

Energy relaxation dynamics in a nodal-line semimetal

Benjamin M. Fregoso,¹ Madhab Neupane,² and Anup Pradhan Sakhya²

¹*Department of Physics, Kent State University, Kent, Ohio 44242, USA*

²*Department of Physics, University of Central Florida, Orlando, Florida 32816, USA*

We study the energy relaxation dynamics in a simple model of a nodal-line semimetal in the presence of an acoustic and an optical phonon branch. In the typically scenario, the temperature relaxation varies linearly as a function of time both at high and low temperatures with rates that could go as $\sim n^{-1/2}$ or n with the electron density in the high-temperature regime or $\sim n^{1/2}$ in the low-temperature regime. To elucidate the role of the nodal line, we compare the relaxation dynamics of a nodal-line semimetal with the relaxation dynamics of Weyl/Dirac semimetals and graphene which have nodal points instead of nodal lines.

I. INTRODUCTION

Electron-phonon interactions give rise to charge density wave and BCS-superconducting instabilities in metals, but at the same time phonons are the main pathway to electronic thermalization.¹⁻⁵ In applications, longer phonon relaxation times are usually associated with more robust quantum behavior while faster relaxation times are usually associated with fast response times in thermal devices.²

Energy relaxation in metals has been extensively studied in the context of pump-probe experiments where the electrons are excited via laser pulses. The details of the temperature decay in time contains information about the electron-phonon coupling constant which determines T_c in BCS superconductors³. This can be contrasted with transport measurements where many relaxation processes play important roles. The temperature relaxation dynamics also carries information about other microscopic processes. For example, at low temperature the phonon cooling power is proportional to the electron and lattice temperature difference $T_e^\kappa - T_L^\kappa$ where $\kappa = 5$ in conventional three-dimensional (3D) metals,^{1,4} 6 in disordered thin films,^{6,7} 3 when phonon phase space is constrained,⁸ and 4 in graphene.⁹

Energy relaxation also contains information about the Fermi surface (FS) of Dirac materials.¹⁰ Graphene is a 2D metal with zero-energy (nodal) points and a small FS which exhibits strong suppression of electron-phonon scattering below the Bloch-Gruneisen temperature^{11,12} and disorder-mediated electron-phonon scattering.^{13,14} Similarly, Weyl/Dirac semimetals have nodal points and exhibit asymmetric Fano line shapes¹⁵ and strong electron-phonon coupling constant.¹⁶

The discovery of nodal-line semimetals^{17,18} (NLSM) adds another member to the family of Dirac materials. NLSMs can be classified by topological invariants¹⁸⁻²⁰ and were demonstrated experimentally in PbTaSe₂,²¹ PtSn₄,²² and ZrSiS^{23,24} with other materials being investigated.^{25,26} NLSMs exhibit unusual magnetoresistance²⁷, strong light-matter interactions,²⁸ correlation-induced reduction of free carrier Drude weight,²⁹ and they are predicted to exhibit quasi-topological electro-magnetic response,³⁰ enhanced excitonic instability,³¹

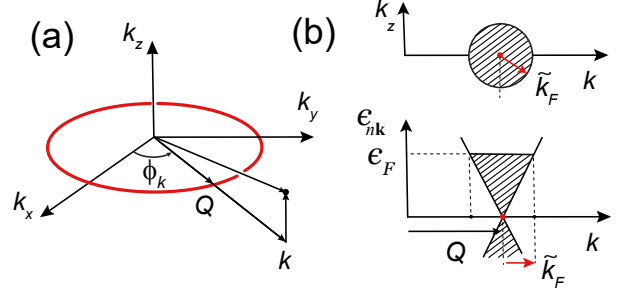


FIG. 1. (a) Nodal line (red ring) in a nodal-line semimetal (NLSM) model. (b) Quasiparticles have linear dispersion near points $(k, \phi_k, k_z) = (Q, \phi_k, 0)$, $0 \leq \phi_k < 2\pi$. In the plane $k-k_z$ the states within radius k_F are occupied and the Fermi surface (FS) is a torus in momentum space.

low coulomb screening,³² and diverging mobility.³³

Here we calculate the electron temperature dynamics in a NLSM after a sudden excitation. We use a simple two-band model consisting of a ring (nodal line) in momentum space, see Fig. 1. An effective Hamiltonian with this dispersion was given in Ref. 18. The main assumptions are: (1) the electrons are in equilibrium among themselves at temperature T_e , (2) the phonons are in equilibrium among themselves at a fixed temperature T_L , and (3) the temperature is higher than the Bloch-Gruneisen temperature (see below).

NLSMs, Weyl/Dirac SMs and graphene all have quasiparticles with linear dispersion near nodal points, but the nodal manifold is 1D in NLSMs and 0D in Weyl SMs and graphene. The main effect of the nodal line is to constrain the electron momenta to values near the nodal line in scattering events. In graphene and Weyl/Dirac SMs, on the other hand, the magnitude of electron momenta can be arbitrarily close to the zone center. As a result, the acoustic phonon cooling power is greatly diminished in NLSMs at high temperature with respect to graphene and Weyl/Dirac SMs. We calculate the temperature as a function of time analytically in the limit of low and high-density, low and high temperature, and small and large optical phonon energy. The forms of the relaxations are summarized in Table I. The typical scenario in pump-probe experiments corresponds to finite

	NLSM	Weyl SM	Graphene
Spatial dimension	3	3	2
Nodal dimension	1	0	0
Optical phonon relaxation			
low density: $\omega_0 \gg T_e \gg T_L, \mu$	inv log eqn. 18	inv log eqn. D6	inv log eqn. 18
low density: $T_e \gg \omega_0, T_L, \mu$	exp 20	1/t D7	exp 20
high density: $\mu, \omega_0 \gg T_e \gg T_L$	inv log 25	inv log D11	inv log 25
high density: $\mu \gg T_e \gg \omega_0, T_L$	lin 27	lin D14	lin 27
Acoustic phonon relaxation			
low density: $T_e \gg T_L, \mu$	exp 30	$1/\sqrt[3]{t}$ †D19	$1/\sqrt{t}$ *E5
low density: $T_e \gtrsim T_L, (\mu = 0)$	exp 30	exp †D19	exp *E5
high density: $\mu \gg T_e \gg T_L$	lin 31	lin †D21	lin *E6
high density: $\mu \gg T_e \gtrsim T_L$	exp 31	exp †D21	exp *E6

TABLE I. Electron temperature as a function of time in NLSMs, graphene, and Weyl SMs in various limits. n : electron density measured from the nodal manifold, T_e : electron temperature, ω_0 : optical phonon energy, μ : chemical potential, T_L : lattice temperature, exp: exponential, lin: linear, inv log: inverse log. *Ref. 34, †Ref. 35, only the tails of the relaxation functions are shown. The reference indicates the relevant equation in the text. For clarity we omit \hbar and k_B .

density and large initial temperature. In this case we find linear relaxation as a function of time in both the high and low-temperature regimes. Linear relaxation is common to all Dirac materials in this regime.

The paper is organized as follows. We first consider optical and acoustic phonon branches separately obtaining analytic solutions in various limits (Secs. II, III and IV). The solutions are then used to give expressions for the crossover temperature between the high- and low-temperature regimes in Sec. V. In Sec. VI we give numerical solutions including both phonon branches and we conclude in Sec. VII. In the appendixes we include some details of the calculations.

II. PHONON COOLING POWER

The basic model is

$$\frac{d\mathcal{E}}{dt} = -\mathcal{P}, \quad (1)$$

where the energy depends on a time-dependent temperature and chemical potential $\mathcal{E}(t) = \mathcal{E}(\mu(t), T_e(t))$. This hydrodynamic approach was used to study transport^{36,37} and cooling^{34,35,38,39} in graphene and other Dirac materials. At not too low temperatures it predicts an inverse root square relaxation in graphene due to acoustic phonon scattering.^{34,38,39} In Weyl SMs it predicts an inverse cubic root³⁵ relaxation due to acoustic phonon scattering. \mathcal{P} is the rate of energy transfer from phonon scattering processes¹

$$\mathcal{P} = \frac{1}{V} \sum_{n\mathbf{k}} \epsilon_{n\mathbf{k}} \frac{df_{n\mathbf{k}}}{dt}, \quad (2)$$

where $\epsilon_{n\mathbf{k}}$ is the quasiparticle energy

$$\epsilon_{n\mathbf{k}} = nv\hbar[k_z^2 + (k - Q)^2]^{1/2}, \quad (3)$$

and $n = 1(-1)$ denotes conduction (valence) band, v is the velocity of nodal quasiparticles, and Q the radius of the nodal ring, see Fig. 1(a). The change in the electron distribution due to phonon scattering is (at the classical level)

$$\begin{aligned} \frac{df_{n\mathbf{k}}}{dt} &= \sum_{m\mathbf{p}} [f_{n\mathbf{k}}(1-f_{m\mathbf{p}})W_{n\mathbf{k},m\mathbf{p}} - (n\mathbf{k} \leftrightarrow m\mathbf{p})], \quad (4) \\ W_{n\mathbf{k},m\mathbf{p}} &= \frac{2\pi}{\hbar} \sum_{\mathbf{q}} M_{\mathbf{q}} [(N_L + 1)\delta_{\mathbf{k},\mathbf{p}+\mathbf{q}}\delta(\epsilon_{n\mathbf{k}} - \epsilon_{m\mathbf{p}} - \hbar\omega_{\mathbf{q}}) \\ &\quad + N_L\delta_{\mathbf{k},\mathbf{p}-\mathbf{q}}\delta(\epsilon_{n\mathbf{k}} - \epsilon_{m\mathbf{p}} + \hbar\omega_{\mathbf{q}})], \quad (5) \end{aligned}$$

where $f_{n\mathbf{k}} \equiv f(\epsilon_{n\mathbf{k}}) = [e^{(\epsilon_{n\mathbf{k}} - \mu)/k_B T_e} + 1]^{-1}$ is the Fermi distribution function, $N_L \equiv N_L(\hbar\omega_{\mathbf{q}}) = [e^{\hbar\omega_{\mathbf{q}}/k_B T_L} - 1]^{-1}$ is the Bose distribution function evaluated at the lattice temperature T_L , T_e is the electron temperature, $M_{\mathbf{q}} = \hbar^2 D^2 q^2 (1 + s_{nm} \cos \theta) / 4\rho V \hbar \omega_{\mathbf{q}}$ is the amplitude of electron-phonon scattering, \mathbf{q} is the phonon momentum, $\omega_{\mathbf{q}}$ the phonon dispersion relation, D the deformation potential of acoustic phonons, ρ the ion mass density, V the volume, θ the angle between \mathbf{k} and \mathbf{p} , and $s_{nm} = 1(-1)$ for intraband (interband) scattering. From Eqn. 4 and 5, Eqn. 2 can be written as^{34,38} (see also appendix A)

$$\mathcal{P} = \frac{2\pi}{V} \sum_{n\mathbf{k}m\mathbf{p}} \omega_{\mathbf{q}} (f_{n\mathbf{k}} - f_{m\mathbf{p}}) (N_L - N_e) M_{\mathbf{q}} \times \delta(\epsilon_{n\mathbf{k}} - \epsilon_{m\mathbf{p}} - \hbar\omega_{\mathbf{q}}) \quad (6)$$

where $\mathbf{q} = \mathbf{p} - \mathbf{k}$. We assume Eqn. 4 does not vanish even for equilibrium distributions of bosons and fermions because they are at distinct temperatures. The nonvanishing Eqn. 6 for $T_e \neq T_L$ is consistent with this assumption.³ The radius of the nodal line Q is taken as the largest momentum scale in the system $Q \gg |k_F - Q|, k_B T_e / v\hbar, \omega_0 / v$ and phonons with momenta $2Q$ can be thermally excited. This requires $k_B T_e > k_B T_{BG} = \hbar c 2Q$, where T_{BG} is the Bloch-Grüneisen temperature.

III. OPTICAL PHONONS

In this section we consider the temperature relaxation in NLSMs due to optical phonons

$$\frac{d\mathcal{E}}{dt} = -\mathcal{P}_o, \quad (7)$$

analytically in various limits. We model the optical phonon with a constant energy dispersion $\omega_{\mathbf{q}} = \omega_0$ and constant electron-phonon matrix element $M_{\mathbf{q}} \equiv g^2/V$. From Eqn. 6 we obtain (see appendix B)

$$\mathcal{P}_o = \frac{g^2 Q^2 \omega_0^4}{2\pi v^4 \hbar} F(N_e - N_L) \quad (8)$$

where $N_e = N_e(\hbar\omega_0)$ and $N_L = N_L(\hbar\omega_0)$ and

$$F(\mu, T_e) \equiv \int_{-\infty}^{\infty} dx |x(x-1)| [f(\hbar\omega_0 x - \hbar\omega_0) - f(\hbar\omega_0 x)]. \quad (9)$$

As seen from the factor in parenthesis in Eqn. 8, \mathcal{P}_o is exponentially suppressed at low temperatures $k_B T_e \ll \hbar\omega_0$, and hence in this regime we expect acoustic phonon scattering to dominate. The energy is a function of $\mu > 0$ and T_e which in turn are functionally related by the constant density condition. In our NLSM model the energy and density are

$$\mathcal{E} = \frac{1}{V} \sum_{n\mathbf{k}} \epsilon_{n\mathbf{k}} f_{n\mathbf{k}} = \frac{v\hbar Q}{2\pi} I_{2+} \quad (10)$$

$$n = \frac{1}{V} \sum_{n\mathbf{k}} f_{n\mathbf{k}} = \frac{Q}{2\pi} I_{1-}, \quad (11)$$

where

$$I_{n\pm} \equiv \int_0^{\infty} \tilde{k}^n d\tilde{k} [f_{c\tilde{k}} \pm (1 - f_{v\tilde{k}})], \quad (12)$$

$\tilde{k} = [k_z^2 + (k - Q)^2]^{1/2}$, $f_{n\tilde{k}} = [e^{\beta(nv\hbar\tilde{k} - \mu)} + 1]^{-1}$, and $\beta \equiv 1/k_B T_e$. The density is measured with respect to the nodal line.

A. Low-density limit

In the low-density limit ($\mu = 0$) the relative size of $\hbar\omega_0$ with respect to $k_B T_e$ gives various relaxation behaviors.

case 1: ($\hbar\omega_0 \gg k_B T_e \gg k_B T_L, \mu$). The situation is illustrated in Fig. 2(a). High-energy electrons at the tail of the distribution lower their energy by emitting optical phonons and dropping to unoccupied states. A rapid thermalization among electrons (not included here) creates a new Fermi distribution at lower temperature. If the energy of the optical phonon is too large, the cooling becomes inefficient. Interestingly, the temperature

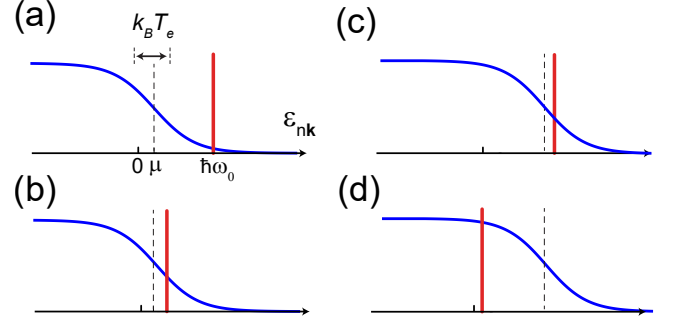


FIG. 2. Electron distribution $f(\epsilon_{n\mathbf{k}})$ at temperature T_e (blue curve) in the limits considered in Sec. III. Also shown are the chemical potential μ (assumed positive) and optical phonon energy $\hbar\omega_0$.

at which optical-phonon cooling stops is not of the order $\hbar\omega_0$ but could be an order of magnitude smaller, see Sec. V.

To begin, note that Eqn. 9 is a function of $\bar{\beta} \equiv \hbar\omega_0/k_B T_e$ and can be integrated analytically in terms of polylogarithm functions. We present the first two terms in the asymptotic expansion of F for large $\bar{\beta}$

$$F(0, T_e) \sim \frac{1}{6} + \frac{6\zeta(3)}{\bar{\beta}^3} + \dots, \quad \bar{\beta} \gg 1 \quad (13)$$

because in this limit we can give an analytic solution. The total time derivative of the energy 2 has a contribution from the density $\partial\mathcal{E}/\partial\mu = 2n$, and a contribution from $\partial\mathcal{E}/\partial T_e$ where

$$\mathcal{E} = \frac{Qk_B^3 T_e^3 3\zeta(3)}{2\pi v^2 \hbar^2} + \frac{Qk_B T_e \log(2)}{\pi v^2 \hbar^2} \mu^2 + \dots \quad \mu \ll k_B T_e \quad (14)$$

$$n = \frac{Qk_B T_e \log(2)}{\pi v^2 \hbar^2} \mu + \dots \quad \mu \ll k_B T_e \quad (15)$$

The contribution from density vanishes in the limit $\mu \rightarrow 0$ and hence $(\partial\mathcal{E}/\partial T_e)(\partial T_e/\partial t) = -\mathcal{P}_o$ (in the variable $\bar{\beta}$) becomes

$$\frac{d\bar{\beta}}{dt} \sim \gamma_{on1} (\bar{\beta}^4 + 36\zeta(3)\bar{\beta} + \dots) e^{-\bar{\beta}}, \quad (16)$$

where we assume $T_e \gg T_L$. The initial condition is $\bar{\beta}_0 = \hbar\omega_0/k_B T_0 \gg 1$ and $\gamma_{on1} = g^2 Q \omega_0 / v^2 \hbar^2 54\zeta(3)$. The right-hand side of Eqn. 16 has a local maximum at $\bar{\beta} \sim 1$ and an exponential tail for large $\bar{\beta}$. In the limit $\bar{\beta} \gg 1$ we obtain an inverse log temperature relaxation

$$\bar{\beta} \sim \log(\gamma_{on1} \bar{\beta}_0^4 t + e^{\bar{\beta}_0}) + 4 \log \frac{T_0}{T_e}, \quad (17)$$

or

$$k_B T_e \sim \frac{\hbar\omega_0}{\log(\gamma_{on1} \bar{\beta}_0^4 t + e^{\bar{\beta}_0})}, \quad (18)$$

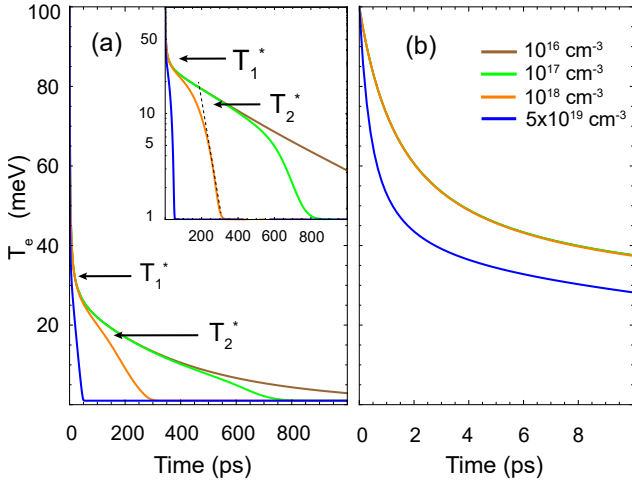


FIG. 3. (a) Electron temperature relaxation in a NLSM with an acoustic and optical phonon branch for various electronic densities. The initial temperature is $T_0 = 100$ meV and the lattice temperature $T_L = 1$ meV. The rest of parameters are in able III. The curves correspond to regime $\hbar\omega_0 \gg k_B T_e$. The time scales are $\tau_a = 50 - 400$ ps, $\tau_o = 1 - 4$ ps for of acoustic and optical phonon relaxations respectively. The brown curve exhibits inverse log \rightarrow exponential behaviors as T_e decreases. The orange curve exhibits inverse log \rightarrow linear \rightarrow exponential behaviors as T_e decreases. T_1^* is the crossover temperature separating the high (optical) and low (acoustic) temperature regimes. T_2^* marks the transition linear \rightarrow exponential. (b) same as (a) but with a smaller time range.

where in the last expression we drop a small (for $T_e \lesssim T_0$) logarithmic correction. The relaxation time scale is $e^{\bar{\beta}_0}/\gamma_{on1}\bar{\beta}_0^4$. Note that $\bar{\beta}$ increases monotonically with time and hence it is enough to request $\bar{\beta}_0 \gg 1$. In fact, even if not initially, the regime $\bar{\beta} \gg 1$ may be eventually reached. However, at lower temperature $T_e < T_1^*$ the system enters a regime dominated by acoustic-phonon scattering and the above considerations do not apply, see Sec. V.

Fig. 3(b) (orange curve) shows an example of a NLSM with $\bar{\beta}_0 = 3$ in the low-density regime. The temperature relaxation is approximately given by Eqn. 18.

case 2: ($k_B T_e \gg \hbar\omega_0, k_B T_L, \mu$). In this regime, there are plenty of electrons with enough energy to emit optical phonons, see Fig. 2(b), and we expect a faster temperature relaxation. In this regime F in Eqn. 9 is approximated by

$$F(0, T_e) = \frac{\pi^2}{3\bar{\beta}^2} - \frac{1}{6} + \frac{\bar{\beta}}{12} - \frac{\bar{\beta}^3}{360} + \dots \quad \bar{\beta} \ll 1 \quad (19)$$

If, in addition, $T_e \gg T_L$, then $N_e(\hbar\omega_0) - N_L(\hbar\omega_0) \sim k_B T_e/\hbar\omega_0 - k_B T_L/\hbar\omega_0 \sim 1/\bar{\beta}$ and to leading order the relaxation is exponential

$$\frac{dT_e}{dt} = -\gamma_{on2} T_e, \quad (20)$$

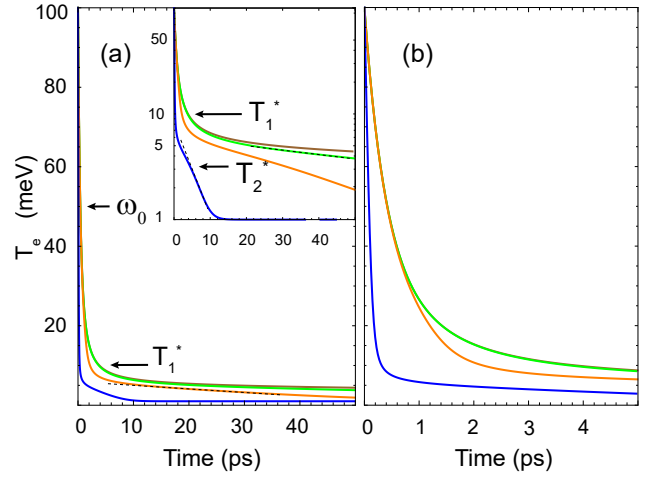


FIG. 4. Same as in Fig. 3 but with $\hbar\omega_0 = 50$ meV, i.e., $\hbar\omega_0 < k_B T_0$. Since optical phonon energies range is 20-50 meV, this regime is the typical situation in pump-probe experiments. The time scales are $\tau_a = 10 - 50$ ps and $\tau_o = .5 - 1$ ps for acoustic and optical phonon relaxations respectively. The green curve exhibits exponential \rightarrow exponential behaviors as T_e decreases. The blue curve exhibits linear \rightarrow linear \rightarrow exponential behavior as T_e decreases.

where $\gamma_{on2} = g^2 Q \omega_0 \pi^2 / v^2 \hbar^2 27 \zeta(3)$ and the relaxation time scale is $1/\gamma_{on2}$. Fig. 4(b) (green curve) shows the relaxation of a NLSM with $\bar{\beta}_0 = 1/2$, i.e., $k_B T_e \gg \hbar\omega_0$. The temperature relaxation is approximately exponential in agreement with Eqn.20.

B. High-density limit

case 1: ($\mu, \hbar\omega_0 \gg k_B T_e \gg k_B T_L$). In this regime, optical phonon scattering may or may not be available. The maximum value of μ is ϵ_F , the chemical potential at zero temperature and hence $\hbar\omega_0$ can be smaller, larger or of the same order as ϵ_F , see Fig. 2(c). If $\mu \ll \hbar\omega_0$, optical phonon scattering is suppressed and a slower relaxation is expected but if $\mu \sim \hbar\omega_0$, a faster relaxation is expected. To start, note that the asymptotic expansion of F for high density

$$F(\mu, T_e) \sim \left(\frac{1}{6} + \frac{2\bar{\mu}^3}{3} \right) + \frac{2\pi^2 \bar{\mu}}{3\bar{\beta}^2} + \dots, \quad \mu \gg k_B T_e \quad (21)$$

can be obtained from the Sommerfeld expansion in variables $\bar{\mu} \equiv \mu/\hbar\omega_0$ and $\bar{\beta} \equiv \hbar\omega_0/k_B T_e$, valid for $\bar{\mu}\bar{\beta} \gg 1$ (or equivalently $\mu \gg k_B T_e$). In this limit

$$\mathcal{E} = \frac{Q}{6\pi v^2 \hbar^2} (\mu^3 + \frac{\pi^2 \mu}{\beta^2} + \dots), \quad \mu \gg k_B T_e \quad (22)$$

$$n = \frac{Q}{4\pi v^2 \hbar^2} (\mu^2 + \frac{\pi^2}{3\beta^2} + \dots), \quad \mu \gg k_B T_e \quad (23)$$

and hence $\mu(T_e) = \epsilon_F - \pi^2 k_B^2 T_e^2 / 6\epsilon_F + \dots$. Also if $\bar{\beta} \gg 1$ then $N_e - N_L \sim e^{-\hbar\omega_0/k_B T_e} - e^{-\hbar\omega_0/k_B T_L} \sim e^{-\bar{\beta}}$ and the equation of motion is

$$\frac{\partial \bar{\beta}}{\partial t} = \tilde{\gamma}_{od1} \bar{\beta}^3 \left(\frac{1}{6} + \frac{2\bar{\mu}^3}{3} + \frac{2\pi^2 \bar{\mu}}{3\bar{\beta}^2} + \dots \right) e^{-\bar{\beta}}. \quad (24)$$

If $\bar{\mu}\bar{\beta} \gg \pi$, the leading behavior is an inverse log function

$$k_B T_e = \frac{\hbar\omega_0}{\log(\gamma_{od1} \bar{\beta}_0^3 t + e^{\bar{\beta}_0})}, \quad (25)$$

where $\gamma_{od1} = 3g^2 Q \omega_0^2 (1/6 + 2\bar{\mu}^3/3) / \pi^2 v^2 \mu \hbar$. The relaxation time scale $e^{\bar{\beta}_0} / \gamma_{od1} \bar{\beta}_0^3$ goes as $\sim n^{1/2}$ for $\bar{\mu} \ll 1$ and as $\sim n^{-1}$ for $\bar{\mu} \gg 1$ with electronic density. The time scale can either increase or decrease with increasing electron density. Fig. 3(b) (blue curve) illustrates the high-density regime in a NLSM with parameters $\bar{\beta}_0 = 3$, $\bar{\mu} \sim \epsilon_F / \hbar\omega_0 \sim 1$ (Table III). The relaxation is approximately given by Eqn. 25.

case 2: ($\mu \gg k_B T_e \gg \hbar\omega_0, k_B T_L$). This case is illustrated in Fig. 2(d). Since $\mu \gg k_B T_e$ we can use Eqn. 21. In addition, if $\bar{\beta} \ll 1$ and $T_e \gg T_L$ then $N_e - N_L \sim 1/\bar{\beta}$ and the equation of motion becomes

$$\frac{d\bar{\beta}}{dt} = \tilde{\gamma}_{od2} \bar{\beta}^2 \left(\frac{1}{6} + \frac{2\bar{\mu}^3}{3} + \frac{2\pi^2 \bar{\mu}}{3\bar{\beta}^2} \dots \right). \quad (26)$$

If $\bar{\mu}\bar{\beta} \gg \pi$, the leading behavior is linear

$$k_B T_e = k_B T_0 - \hbar\omega_0 \gamma_{od2} t, \quad (27)$$

where the rate $\gamma_{od2} = 3g^2 Q \omega_0^2 (1/6 + 2\bar{\mu}^3/3) / \pi^2 v^2 \hbar \mu$ goes as $\sim n^{-1/2}$ for $\bar{\mu} \ll 1$ or as $\sim n$ for $\bar{\mu} \gg 1$ with electron density, i.e., it can increase or decrease with increasing density. Fig. 4(b) (blue or orange curve) illustrates the high-density regime in a NLSM with $\bar{\beta}_0 = 1/2$. The relaxation is approximately linear for temperatures above ~ 20 meV, see Eqn. 27.

IV. ACOUSTIC PHONONS

In this section we consider the cooling power of acoustic phonons

$$\frac{d\mathcal{E}}{dt} = -\mathcal{P}_a, \quad (28)$$

analytically in a NLSM in various limits. To obtain analytical expressions, we evaluate Eqn. 6 to lowest order in $c/v \ll 1$ where c is the sound speed, assumed isotropic. In this limit, energy relaxation is quasielastic and we obtain (see appendix C)

$$\mathcal{P}_a = \frac{D^2 Q^4 k_B}{4\pi \rho v^2 \hbar} I_{1+}(T_e - T_L). \quad (29)$$

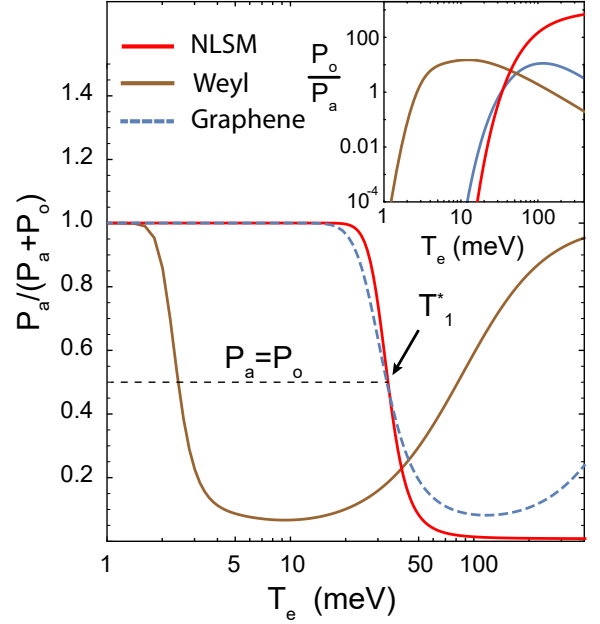


FIG. 5. Percentage of acoustic phonon cooling power as a function of electron temperatures for NLSM, graphene and a Weyl SM. Parameters given in Table III

A. Low-density limit

Setting $\mu = 0$ and using Eqns. 14, 15, and 29 we obtain

$$\frac{dT_e}{dt} = -\gamma_{an}(T_e - T_L), \quad (30)$$

where $\gamma_{an} = \pi^2 D^2 Q^3 / \rho v^2 \hbar 108 \zeta(3)$. Hence, the temperature relaxes exponentially with time scale $1/\gamma_{an}$. This can be compared with $\sim 1/\sqrt{t}$ power law found in graphene³⁴ which has nodal points instead of nodal lines and $\sim 1/\sqrt[3]{t}$ power law found in Weyl nodes³⁵. Fig. 3(a) (brown curve) illustrates the low-density regime of a NLSM. The exponential dependence is evident in the log plot inset for $T_e < T_1^*$.

B. High-density limit

In this limit, we can use Eqns. 22, 23, and 29 to obtain

$$\frac{d}{dt}(k_B T_e) = -\gamma_{ad} \frac{1}{T_e} (T_e - T_L), \quad (31)$$

where $\gamma_{ad} = 3D^2 Q^3 \epsilon_F / 4\pi^2 \rho \hbar v^2$. Like in graphene, the relaxation is linear for $T_e \gg T_L$, but unlike in graphene (where $\gamma_{ad} \sim n^{3/2}$)³⁴ the relaxation rate in NLSM goes as $\gamma_{ad} \sim n^{1/2}$ with electron density. The relaxation is exponential for $T_e \gtrsim T_L$ with time scale T_L / γ_{ad} .

Fig. 3(a) (orange or blue curve) shows the temperature relaxation in the high-density regime of a NLSM. The appearance of a linear relaxation for temperatures $T_1^* > T > T_2^*$ is evident in the figure and is in agreement with Eqn. 31. There is an exponential relaxation for $T < T_2^*$.

V. CROSSOVER TEMPERATURE

The temperature at which the optical phonon cooling power equals the acoustic phonon cooling power

$$\mathcal{P}_a(T_1^*) = \mathcal{P}_o(T_1^*), \quad (32)$$

defines the boundary between the regime dominated by optical phonons ($> T_1^*$) and the regime dominated by acoustic phonons ($< T_1^*$). If the initial temperature is $T_0 > T_1^*$, the decay is initially fast followed by a slower decay. If $T_0 < T_1^*$, the decay is slower and the electron plasma is longer lived. Hence, an estimate of the crossover temperature is important for experimental design, e.g., pump-probe experiments or device design, and also as a control knob in probing microscopic mechanisms in materials. We consider two limiting cases.

A. Low-density limit

case 1: ($\hbar\omega_0 \gg k_B T_e \gg k_B T_L, \mu$). From Eqns. 8, 13, and 29 we find that $\bar{\beta}^* = \hbar\omega_0/k_B T_1^*$ satisfies

$$\alpha_1 \equiv \frac{\pi^2 D^2 Q^2 \hbar}{2\rho g^2 \omega_0} = [(\bar{\beta}^*)^3 + 36\zeta(3)]e^{-\bar{\beta}^*}. \quad (33)$$

The left hand side is a constant that depends on materials' properties. The right-hand side depends on $\bar{\beta}^*$. The intersection of the two gives the solution. Note that if $\alpha_1 < 36\zeta(3)$ and $\bar{\beta}^* \gg 1$ there is a solution.

case 2: ($k_B T_e \gg \hbar\omega_0, k_B T_L, \mu$). From Eqns. 8, 19, and 29 we find that $\bar{\beta}^* = \hbar\omega_0/k_B T_1^*$ satisfies

$$\alpha_1 = 2\pi^2 - \bar{\beta}^{*2} + \frac{\bar{\beta}^{*3}}{2} + \dots. \quad (34)$$

There is a solution when $\alpha_1 < 2\pi^2$ and $\bar{\beta}^* \ll 1$.

B. High-density limit

case 1: ($\mu, \hbar\omega_0 \gg k_B T_e \gg k_B T_L$). From Eqn. 8, 21, and 29 we find that $\bar{\beta}^* = \hbar\omega_0/k_B T_1^*$ satisfies

$$\alpha_2 \equiv \frac{3D^2 Q^2 \mu^2}{2\rho g^2 \omega_0^3 \hbar} = [\bar{\beta}^*(1 + 4\bar{\mu}^3) + 4\pi^2 \frac{\bar{\mu}}{\bar{\beta}^*}]e^{-\bar{\beta}^*}. \quad (35)$$

A graphical solution for a NLSM in the high-density regime is shown in Fig. 6. Using the parameters in Table III, we obtain $\alpha_2 = 0.0042$ and $k_B T_1^* = \hbar\omega_0/\bar{\beta}^* = 34$ meV which is close to the full numerical solution $k_B T_1^* = 35$ meV shown in Fig. 5.

case 2: ($\mu \gg k_B T_e \gg \hbar\omega_0, k_B T_L$). From Eqns. 8, 21, 29 and $N_e - N_L \sim 1/\bar{\beta}$ we find

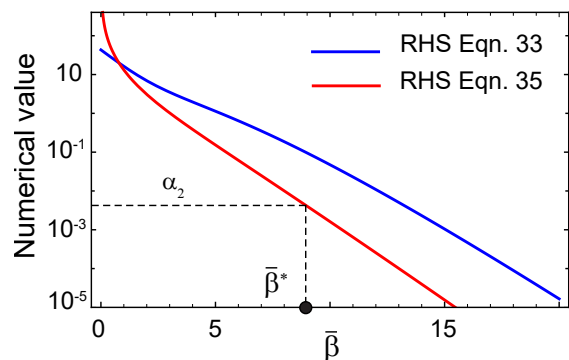


FIG. 6. Solution of Eqn. 35 for the crossover temperature T_1^* of our NLSM model. The red curve is the right-hand side (RHS) of 35 and the blue curve the RHS of 33. Parameters are taken from Table III. The crossover temperature is $k_B T_1^* = \hbar\omega_0/\bar{\beta}^* = 34$ meV which compares well with exact numerical solution ~ 35 meV, see Fig. 5.

$$k_B T_1^* = \frac{DQ\hbar}{2\pi g} \left(\frac{3\mu}{2\rho} \right)^{1/2} \sim n^{1/4}. \quad (36)$$

VI. NUMERICAL SOLUTION

In this section, we solve numerically for the energy relaxation dynamics due to acoustic and optical phonons

$$\frac{d\mathcal{E}}{dt} = -\mathcal{P}_a - \mathcal{P}_o, \quad (37)$$

subject to constant density. From Eqns. 2, 8, and 29 μ and T_e obey the differential equation

$$\begin{aligned} -3QT_e v \hbar \left(\frac{\partial}{\partial t} \frac{1}{T_e} \right) I_{2+} + 2QT_e \left(\frac{\partial}{\partial t} \frac{\mu}{T_e} \right) I_{1-} = \\ - \frac{D^2 Q^4 k_B}{4\pi \rho v^2 \hbar} I_{1+} (T_e - T_L) - \frac{g^2 Q^2 \omega_0^4}{2\pi v^4 \hbar} F (N_e - N_L), \end{aligned} \quad (38)$$

which together with Eqn. 11 and the initial conditions $\mu(t=0) = \mu_0$ and $T_e(t=0) = T_0$ completely determine the subsequent evolution. Fig. 3 shows the electron temperature as a function of time for a NLSM with parameters given in Table III. The initial temperature is $T_0 = 100$ meV = 1200 K. Note a sharp change in behavior at temperature T_1^* . For $T_e > T_1^* \sim 35$ meV (high-temperature regime), there is a fast relaxation associated with optical phonons. This is because at these temperatures $\mathcal{P}_a \ll \mathcal{P}_o$, see Fig. 5. For $T_e < T_1^*$ (low-temperature regime) acoustic phonons saturate the cooling power and hence dominate the relaxation process. In the high-temperature regime the relaxation time scale

is picoseconds, but in the low-temperature regime, the relaxation time scale is nanoseconds. As expected, the optical phonon relaxation is faster than acoustic phonon relaxation.¹

Note that the higher the density, the faster the relaxation. In the high-temperature regime at any density, the relaxation is of the inverse log form as indicated in Eqn. 18 or Eqn. 25 even though β_0 is only 3. In the low-temperature low-density regime, the relaxation is exponential for $T_e < T_1^*$ (brown curve Eqn. 30) and linear-exponential (orange curve) in the high-density regime (Eqn. 31). The relaxation time scale depends weakly on density at high temperatures and strongly at low temperatures. Although not shown, the chemical potential increases monotonically towards ϵ_F as time increases.

Note that in the high-temperature regime \mathcal{P}_a is very low in NLSMs but sizable in a Weyl SMs and graphene, see Fig. 5. In fact, there is a clean separation of scattering processes in the high and low-temperature regimes in NLSMs which justifies considering optical and phonon scattering separately in Secs. III and IV.

Fig. 4 shows the relaxation of a NLSM in the regime $k_B T_e \gg \hbar\omega_0$. Since emission of optical phonons is readily available we expect a faster relaxation as shown in the figure.

VII. DISCUSSION AND CONCLUSIONS

We calculated the electron temperature relaxation as a function of time after a sudden excitation in a simple model of a NLSM with an acoustic and optical branch. The main assumptions are (1) the electrons are in equilibrium with themselves at a temperature T_e , (2) phonons are in thermal equilibrium with themselves at a fixed temperature T_L , and (3) phonons of large momenta $> 2Q$ can be thermally excited, i.e., $k_B T_e > \hbar c 2Q \equiv k_B T_{BG}$. If we consider the values $c = 4.3\text{--}6.8$ km/s and $Q \sim .3 \text{ \AA}^{-1}$ for ZrSiS⁴⁰ then $k_B T_{BG} = 17\text{--}26$ meV = 197 – 300 K. If $T_L < T_{BG}$, the electron plasma eventually enters the Bloch-Gruneisen regime as it cools down and our results do not apply in this regime. Under these assumptions, we obtained various relaxation behaviors analytically in the high and low-temperature regimes summarized in Table I.

The role of the nodal line in the NLSM is evident in the low-temperature (acoustic) low-density regime where the NLSM, the Weyl SM and graphene have very different relaxation behaviors, namely, exponential, $t^{-1/3}$, and $t^{-1/2}$ respectively. The equation of motion $C dT_e/dt = -\mathcal{P}_a$ with the heat capacity $\mathcal{C} = d\mathcal{E}(\mu(T_e), T_e)/dT_e$ implies that κ in

$$\frac{dT_e}{dt} \sim -T_e^\kappa (T_e - T_L) \quad (39)$$

is given by $\kappa = \dim \mathcal{P}_a - \dim \mathcal{C}$ or

$$\kappa = (2(\mathcal{D} - d) - 1 + 2[q] - 1) - (\mathcal{D} - d + a - 1). \quad (40)$$

	NLSM	Weyl	Graphene
\mathcal{D}	3	3	2
d	1	0	0
$2[q]$	0	2	2
$\dim \mathcal{C}$	2	3	2
$\dim \mathcal{P}_a$	2	6	4
$\dim \mathcal{P}_a - \dim \mathcal{C}$	0 [†]	3 [*]	2 ^{††}

TABLE II. Temperature scales of Dirac materials see Sec. VII: \mathcal{D} spatial dimension, d nodal manifold dimension, $\dim \mathcal{C}$ scale dimension of the heat capacity, $\dim \mathcal{P}_a$ scale dimension of acoustic cooling power. [†] Eqn. 30, ^{*} Eqn. D19, ^{††} Eqn. E5.

To obtain $\dim \mathcal{C}$, we can inspect Eqn. 10. First subtract d nodal (frozen) directions from \mathcal{D} spatial dimensions and add the power of the quasiparticle dispersion a (1 in this case). The temperature derivative of the energy gives the last -1. The electronic heat capacity scales as T_e with a power of 3 in Weyl node and with a power of 2 in graphene and NLSMs. In this sense NLSMs and graphene are similar.

To obtain $\dim \mathcal{P}_a$, we can inspect Eqn. 6. We have $2(\mathcal{D} - d)$ powers from the integrals, subtract 1 from the energy conservation, and add 2 if momentum transfer $[q]$ is not constrained, i.e., in Weyl nodes and graphene. Finally, subtract 1 from the Fermi function differences. The last two steps occur because we expanded the integrals to lowest order in c/v . The role of the nodal line is now explicit. From Eqn. 40, $\dim \mathcal{P}_a = 6$ for Weyl SMs, 4 for graphene and 2 for NLSMs, see Table II. It is the lowest for NLSM. The large decrease in \mathcal{P}_a in a NLSM at high temperature is because the electron momenta are fixed near the nodal ring in electron-phonon scattering processes whereas in a Weyl SM or graphene the electron momenta can take any value along the radial direction. For this reason, the high-temperature regime is dominated by optical phonon emission in NLSMs but not in Weyl SMs and graphene, see Fig. 5. In conclusion, a combination of phonon scattering dynamics and to a lesser extent of energetics gives the exponential relaxation ($\kappa = 0$) in NLSMs and a power laws in graphene ($\kappa = 2$) and in Weyl SMs ($\kappa = 3$).

We have considered a simplified model of a NLSM consisting of ring in momentum space with cylindrical symmetric, particle-hole symmetry and time reversal symmetry. Our conclusions will not change if the orientation of the ring changes as long as there is rotational symmetry about its axes. Particle-hole symmetry ensures the ring is evenly filled. If particle-hole symmetry or cylindrical symmetry is broken by a small amount, our results are approximate. If there is more than one ring or if we consider the spin of the electrons, the total cooling power is multiplied by the number of equivalent rings or by the spin degeneracy.

	NLSM	Weyl	Graphene
ρ (kg/m ³ , kg/m ²)	4.86 †	12.03	3.7×10^{-7}
n (cm ⁻³ , cm ⁻²)	5×10^{19}	10^{14}	10^{13}
ϵ_F (meV)	300	6	370
Q (1/Å)	.3	-	-
$\hbar\omega_0$ (meV)	300	31	196
D (eV)	5	4	20
v (10 ⁶ m/s)	1	.5	1
a (Å)	4	6.3	1.42
g ($v\hbar^2/a^2\sqrt{\rho\hbar\omega_0}$)	56.6	4.2	1.4
T_L (meV)	1	1	1

TABLE III. Parameters of a prototypical NLSM from Ref. 40, a Weyl SM, and doped graphene. The electron-phonon coupling constants for NLSMs are unknown. For a Weyl SM we take the known parameters of a single node in TaAs.¹⁰

VIII. ACKNOWLEDGMENTS

BMF acknowledges support from NSF grant DMR-2015639 and DOE-NERSC under contract DE-AC02-05CH11231. M.N. is supported by the Air Force Office of Scientific Research under Award No. FA9550-17-1-0415 and the Air Force Office of Scientific Research MURI (FA9550-20-1-0322).

Appendix A: Phonon cooling power

From Eqn. 2, 4, and 5 we obtain

$$\mathcal{P} = \frac{1}{V} \sum_{n\mathbf{k}} \sum_{m\mathbf{p}} (\epsilon_{n\mathbf{k}} - \epsilon_{m\mathbf{p}}) f_{n\mathbf{k}} (1 - f_{m\mathbf{p}}) W_{n\mathbf{k}, m\mathbf{p}} \quad (\text{A1})$$

$$= \mathcal{P}_1 + \mathcal{P}_2, \quad (\text{A2})$$

where

$$\mathcal{P}_1 = \frac{2\pi}{\hbar} \frac{1}{V} \sum_{n\mathbf{k}} \sum_{m\mathbf{p}} (\epsilon_{n\mathbf{k}} - \epsilon_{m\mathbf{p}}) (f_{n\mathbf{k}} - f_{m\mathbf{p}}) M_{\mathbf{q}} N_L \times \delta(\epsilon_{n\mathbf{k}} - \epsilon_{m\mathbf{p}} - \hbar\omega_{\mathbf{q}}) \quad (\text{A3})$$

$$\mathcal{P}_2 = \frac{2\pi}{\hbar} \frac{1}{V} \sum_{n\mathbf{k}} \sum_{m\mathbf{p}} (\epsilon_{n\mathbf{k}} - \epsilon_{m\mathbf{p}}) f_{n\mathbf{k}} (1 - f_{m\mathbf{p}}) M_{\mathbf{q}} \times \delta(\epsilon_{n\mathbf{k}} - \epsilon_{m\mathbf{p}} - \hbar\omega_{\mathbf{q}}). \quad (\text{A4})$$

We assumed $\omega_{-\mathbf{q}} = \omega_{\mathbf{q}}$ which holds for time reversal symmetric systems or inversion symmetric systems. Using the identity

$$f_{n\mathbf{k}} (1 - f_{m\mathbf{p}}) \delta(\epsilon_{n\mathbf{k}} - \epsilon_{m\mathbf{p}} - \hbar\omega_{\mathbf{q}}) = -(f_{n\mathbf{k}} - f_{m\mathbf{p}}) N_e(\hbar\omega_{\mathbf{q}}) \delta(\epsilon_{n\mathbf{k}} - \epsilon_{m\mathbf{p}} - \hbar\omega_{\mathbf{q}}), \quad (\text{A5})$$

\mathcal{P}_2 becomes

$$\begin{aligned} \mathcal{P}_2 &= -\frac{2\pi}{\hbar} \frac{1}{V} \sum_{n\mathbf{k}} \sum_{m\mathbf{p}} (\epsilon_{n\mathbf{k}} - \epsilon_{m\mathbf{p}}) (f_{n\mathbf{k}} - f_{m\mathbf{p}}) M_{\mathbf{q}} N_e \\ &\quad \times \delta(\epsilon_{n\mathbf{k}} - \epsilon_{m\mathbf{p}} - \hbar\omega_{\mathbf{q}}) \\ &\equiv -\mathcal{P}_1(L \rightarrow e). \end{aligned} \quad (\text{A6})$$

This relation (noted in Ref. 38) means Eqn. 2 becomes

$$\mathcal{P} = \frac{2\pi}{V\hbar} \sum_{n\mathbf{k}m\mathbf{p}} (\epsilon_{n\mathbf{k}} - \epsilon_{m\mathbf{p}}) (f_{n\mathbf{k}} - f_{m\mathbf{p}}) (N_L - N_e) M_{\mathbf{q}} \times \delta(\epsilon_{n\mathbf{k}} - \epsilon_{m\mathbf{p}} - \hbar\omega_{\mathbf{q}}), \quad (\text{A7})$$

which is Eqn. 6 in the main text.

Appendix B: Optical phonon cooling in NLSMs

Calculation of \mathcal{P}_o . We start from Eqns. A3 and set $M_{\mathbf{q}} = g^2/V$, $\omega_{\mathbf{q}} = \omega_0$ to obtain

$$\mathcal{P}_{o1} = 2\pi g^2 N_L \omega_0 \frac{1}{V^2} \sum_{n\mathbf{k}} \sum_{m\mathbf{p}} (f_{n\mathbf{k}} - f_{m\mathbf{p}}) \delta(\epsilon_{n\mathbf{k}} - \epsilon_{m\mathbf{p}} - \hbar\omega_0). \quad (\text{B1})$$

Now we write the sums over momenta as integrals in cylindrical coordinates and define $k' \equiv k - Q$. The integral over k' is now from $-Q$ to ∞ . Now extend the integration over k' to the whole real line and parameterized the plane k', k_z in terms of polar coordinates $\tilde{k}, \phi_{\tilde{k}}$ to obtain

$$\begin{aligned} \mathcal{P}_{o1} &= g^2 N_L \omega_0 \frac{1}{(2\pi)^3} \sum_{nm} \int \tilde{k} d\tilde{k} d\phi_{\tilde{k}} \int \tilde{p} d\tilde{p} d\phi_{\tilde{p}} \\ &\quad \times (\tilde{k} \sin \phi_{\tilde{k}} + Q) (\tilde{p} \sin \phi_{\tilde{p}} + Q) [f(nv\hbar\tilde{k}) - f(mv\hbar\tilde{p})] \\ &\quad \times \delta(\epsilon_{n\tilde{k}} - \epsilon_{m\tilde{p}} - \hbar\omega_0) \quad (\text{B2}) \\ &= g^2 N_L \omega_0 \frac{Q^2}{2\pi v\hbar} \sum_{nm} \int \tilde{k} d\tilde{k} \int \tilde{p} d\tilde{p} \\ &\quad \times [f(nv\hbar\tilde{k}) - f(mv\hbar\tilde{p})] \delta(n\tilde{k} - m\tilde{p} - \omega_0/v), \quad (\text{B3}) \end{aligned}$$

where in the last equality we use the fact that the delta function fixes $m\tilde{p} = n\tilde{k} + \omega_0/v$ and that the Fermi-function difference is very small for $\tilde{k} \gg \omega_0/v$. This justifies extending the limits of integrals of \tilde{k} and \tilde{p} to the whole real line as long as $Q \gg \omega_0/v, k_B T_e/v\hbar$. After some algebra

$$\mathcal{P}_{o1} = -\frac{g^2 \omega_0^4 Q^2}{2\pi v^4 \hbar} F N_L, \quad (\text{B4})$$

where F is given by Eqn. 9. Finally $\mathcal{P}_o = \mathcal{P}_{o1}(L) - \mathcal{P}_{o1}(L \rightarrow e)$ gives Eqn. 8 in the main text.

Appendix C: Acoustic phonon cooling in NLSMs

Calculation of \mathcal{P}_a . Starting from Eqn. A3 substitute $M_{\mathbf{q}}, \omega_{\mathbf{q}} = cq = c|\mathbf{k} - \mathbf{p}|$ and assume the lattice temperature is such that $k_B T_L \gg \hbar\omega_{\mathbf{q}}$. This requires $T_L > T_{BG}$. We obtain

$$\mathcal{P}_a = \frac{2\pi D^2 k_B T_L}{4\rho V^2 c^2} \sum_{n\mathbf{k}} \sum_{m\mathbf{p}} \omega_{\mathbf{q}} (f_{n\mathbf{k}} - f_{m\mathbf{p}}) \times (1 + s_{nm} \cos \theta) \delta(\epsilon_{n\mathbf{k}} - \epsilon_{m\mathbf{p}} - \hbar\omega_{\mathbf{q}}) \quad (\text{C1})$$

Now we write the sums over momenta as integrals in cylindrical coordinates and define $k' = k - Q$. The integral over k' is now from $-Q$ to ∞ . The Fermi functions limit the size of k' to values near $|k_F - Q| \ll Q$. Hence, we can extend the limits of integration of the radial component k' to the whole real line with small error as long as $Q \gg |k_F - Q|, k_B T_e$. Now transform k', k_z variables to polar coordinates $\tilde{k}, \phi_{\tilde{k}}$. In terms of these variables $k' = \tilde{k} \sin \phi_{\tilde{k}}, k_z = \tilde{k} \cos \phi_{\tilde{k}}$ and the dispersion relation $\epsilon_{n\mathbf{k}}$ is that of a Dirac cone in 2D. The energy difference becomes $\epsilon_{n\mathbf{k}} - \epsilon_{m\mathbf{p}} = v\hbar(n\tilde{k} - m\tilde{p})$ and the delta function

$$\delta(\epsilon_{n\mathbf{k}} - \epsilon_{m\mathbf{p}} - \hbar\omega_{\mathbf{q}}) = \frac{1}{v\hbar} \delta(n\tilde{k} - m\tilde{p} - r q) \quad (\text{C2})$$

$$= \frac{1}{v\hbar} \delta_{nm} \delta(\tilde{p} - \tilde{p}_0) [1 + O(r)] \quad (\text{C3})$$

fixes \tilde{p} to $\tilde{p}_0 = \tilde{k} - nr[q]_{\tilde{p}=\tilde{k}}$ (to first order in $r = c/v$). $[q]_{\tilde{p}=\tilde{k}}$ is the phonon momentum to zero order, i.e., equal to $q = |\mathbf{k} - \mathbf{p}|$ with $\tilde{p} = \tilde{k}$. In the limit $Q \gg \tilde{k}_F$

$$q^2 \approx 2Q^2(1 - \cos \phi) \quad (\text{C4})$$

$$1 + s_{nm} \cos \theta \approx 1 + s_{nm} \cos \phi, \quad (\text{C5})$$

where $\phi \equiv \phi_{\mathbf{k}} - \phi_{\mathbf{p}}$. This means the phonon momentum is effectively 2D in the plane $k_x - k_y$. Finally, we note $\hbar\omega_{\mathbf{q}}$ and the Fermi function difference are both $O(r)$ and hence we can set $\tilde{p} = \tilde{k}$ in the rest of the factors of Eqn. C1. Note that

$$f_{n\tilde{k}} - f_{n\tilde{p}} = nr\tilde{q} \frac{\partial f_{n\tilde{k}}}{\partial \tilde{k}} + O(r^2) \quad (\text{C6})$$

is peaked at $\tilde{k} \sim \tilde{k}_F$. As a result Eqn. C1 becomes

$$\mathcal{P}_a = -\frac{D^2 Q^4 k_B}{4\pi \rho v^2 \hbar} I_{1,+} T_L \quad (\text{C7})$$

where

$$I_{n\pm} \equiv \int_0^\infty \tilde{k}^n d\tilde{k} [f_{c\tilde{k}} \pm (1 - f_{v\tilde{k}})] \quad (\text{C8})$$

and $f_{n\tilde{k}} = [e^{(nv\hbar\tilde{k} - \mu)\beta} + 1]^{-1}$

Appendix D: Phonon cooling power in a Weyl node

The quasiparticle energy near a Weyl node is $\epsilon_{n\mathbf{k}} = nv\hbar k$ where $k = |\mathbf{k}|$ is the magnitude of a 3D momentum and $n = \pm 1$ denotes the conduction (+1) and valence band (-1). The FS is a sphere in momentum space.

1. Optical phonons

Following the steps outlined in Appendix B the cooling power of optical phonons in a Weyl node is

$$\mathcal{P}_{wo} = \frac{\omega_0^6 g^2}{v^6 \hbar^2 \pi^3} H(N_e - N_L), \quad (\text{D1})$$

where

$$H \equiv \int_{-\infty}^{\infty} dx x^2 (x-1)^2 [f(\hbar\omega_0 x - \hbar\omega_0) - f(\hbar\omega_0 x)] = \frac{1}{30} + \bar{\mu}^4 + \frac{2\pi^2 \bar{\mu}^2}{\beta^2} + \frac{7\pi^4}{15\beta^4}, \quad (\text{D2})$$

has a simple closed form valid in all regimes of $\bar{\beta} \equiv \hbar\omega_0/k_B T_e$ and $\bar{\mu} \equiv \mu/\hbar\omega_0$.

a. Low-density limit

case 1: ($\hbar\omega_0 \gg k_B T_e \gg T_L, \mu$). If $\bar{\beta} \gg 1$ and $T_e \gg T_L$ then $N_e - N_L \sim e^{-\bar{\beta}}$. The energy and density

$$\mathcal{E} = \frac{v\hbar I_{3+}}{2\pi^2} = \frac{k_B^4 T_e^4 7\pi^2}{120v^3 \hbar^3} + \frac{k_B^2 T_e^2 \mu^2}{4v^3 \hbar^3} + \dots \quad \mu \ll k_B T_e \quad (\text{D3})$$

$$n = \frac{I_{2-}}{2\pi^2} = \frac{k_B^3 T_e^3 \mu}{6v^3 \hbar^3} + \dots \quad \mu \ll k_B T_e, \quad (\text{D4})$$

together with Eqn. D2 and $d\mathcal{E}/dt = -\mathcal{P}_{wo}$ give

$$\frac{d\bar{\beta}}{dt} = \tilde{\gamma}_{won1} (\bar{\beta}^5 + 14\pi^4 \bar{\beta}) e^{-\bar{\beta}}. \quad (\text{D5})$$

To leading order as $\bar{\beta} \gg 1$ the relaxation is an inverse log

$$k_B T_e = \frac{\hbar\omega_0}{\log(\gamma_{won1} \bar{\beta}_0^5 t + e^{\bar{\beta}_0})}, \quad (\text{D6})$$

where $\bar{\beta}_0 \equiv \hbar\omega_0/k_B T_0 \gg 1$, $\gamma_{won1} = g^2 \omega_0^2 / 14\pi^5 v^3 \hbar^2$, and the relaxation time scale is $e^{\bar{\beta}_0} / \gamma_{won1} \bar{\beta}_0^5$.

case 2: ($k_B T_e \gg \hbar\omega_0, T_L, \mu$). In this limit $N_e - N_L \sim 1/\bar{\beta}$ and hence to leading order

$$k_B T_e = \frac{\hbar\omega_0}{\gamma_{won2} t + \bar{\beta}_0}, \quad (\text{D7})$$

where $\gamma_{won2} = g^2 \omega_0^2 / \pi^3 v^3 \hbar^2$.

b. High-density limit

case 1: ($\mu, \hbar\omega_0 \gg k_B T_e \gg T_L$). In the limit of large chemical potential $\mu \gg k_B T_e$ the energy and density are

$$\mathcal{E} = \frac{1}{8\pi^2 v^3 \hbar^3} \left(\mu^4 + \frac{2\pi^2 \mu^2}{\beta^2} + \dots \right) \quad \mu \gg k_B T_e \quad (\text{D8})$$

$$n = \frac{1}{6\pi^2 v^3 \hbar^3} \left(\mu^3 + \frac{\pi^2 \mu}{\beta^2} + \dots \right) \quad \mu \gg k_B T_e. \quad (\text{D9})$$

The last equation implies $\mu(T_e) = \epsilon_F - \pi^2 k_B^2 T_e^2 / 3\epsilon_F + \dots$ and together with $N_e - N_L \sim e^{-\bar{\beta}}$ and Eqn. D2 give

$$\frac{\partial \bar{\beta}}{\partial t} = \tilde{\gamma}_{wod1} \bar{\beta}^3 \left(\frac{1}{30} + \bar{\mu}^4 + \frac{2\pi^2 \bar{\mu}^2}{\bar{\beta}^2} + \frac{7\pi^4}{15\bar{\beta}^4} \right) e^{-\bar{\beta}}. \quad (\text{D10})$$

If $\bar{\mu} \bar{\beta} \gg \pi\sqrt{2}$ the leading behavior is given by the first two terms on the right and we obtain

$$k_B T_e = \frac{\hbar\omega_0}{\log(\gamma_{wod1} \bar{\beta}_0^3 t + e^{\bar{\beta}_0})}, \quad (\text{D11})$$

with $\gamma_{wod1} = 3g^2 \omega_0^4 (1/30 + \bar{\mu}^4) / \pi^2 v^3 \mu^2$ and time scale $e^{\bar{\beta}_0} / \gamma_{wod1} \bar{\beta}_0^3$. The time scale goes as $\sim n^{2/3}$ for $\bar{\mu} \ll 1$ and as $\sim n^{-2/3}$ for $\bar{\mu} \gg 1$.

case 2: ($\mu \gg k_B T_e \gg \hbar\omega_0, T_L$). In this case $N_e - N_L \sim 1/\bar{\beta}$ and from Eqns. D2, D8, and D9 we obtain

$$\frac{d\bar{\beta}}{dt} = \tilde{\gamma}_{wod2} \bar{\beta}^2 \left(\frac{1}{30} + \bar{\mu}^4 + \frac{2\pi^2 \bar{\mu}^2}{\bar{\beta}^2} + \frac{7\pi^4}{15\bar{\beta}^4} \right). \quad (\text{D12})$$

If $\bar{\mu} \bar{\beta} \gg \pi\sqrt{2}$ the leading behavior is

$$\frac{d\bar{\beta}}{dt} = \gamma_{wod2} \bar{\beta}^2, \quad (\text{D13})$$

or

$$k_B T_e = k_B T_0 - \hbar\omega_0 \gamma_{wod2} t, \quad (\text{D14})$$

where the relaxation rate $\gamma_{wod2} = 3g^2 \omega_0^4 (1/30 + \bar{\mu}^4) / \pi^2 v^3 \mu^2$ goes as $\sim n^{-2/3}$ for $\bar{\mu} \ll 1$ and as $\sim n^{2/3}$ for $\bar{\mu} \gg 1$.

2. Acoustic phonons

The cooling power of acoustic phonons in a Weyl SM was studied in Ref. 35. Here we reproduce their results for comparison. Following the same steps as in Appendix C we obtain

$$\mathcal{P}_{wa1} = -\frac{D^2 k_B}{\hbar \rho v^2 \pi^3} I_{5+} T_L \quad (\text{D15})$$

and hence the cooling power of acoustic phonons is³⁵

$$\begin{aligned} \mathcal{P}_{wa} &= \mathcal{P}_{wa1}(L) - \mathcal{P}_{wa1}(L \rightarrow e) \\ &= \frac{D^2 k_B}{\rho v^2 \hbar \pi^3} I_{5+}(T_e - T_L) \end{aligned} \quad (\text{D16})$$

where

$$I_{n\pm} \equiv \int_0^\infty k^n dk [f_{ck} \pm (1 - f_{vk})], \quad (\text{D17})$$

and $f_{nk} = [e^{\beta(nv\hbar k - \mu)} + 1]^{-1}$.

a. Low-density limit

If $\mu = 0$ we can integrate D16 analytically to obtain

$$\mathcal{P}_{wa} = \frac{D^2 k_B^7 T_e^6 31\pi^3}{\rho v^8 \hbar^7 126} (T_e - T_L). \quad (\text{D18})$$

The energy and density of a Weyl node are given by Eqns. D3 and D4 and together with $d\mathcal{E}/dt = -\mathcal{P}_{wa}$ we obtain

$$\frac{dT_e}{dt} = -\gamma_{wan} T_e^3 (T_e - T_L) \quad (\text{D19})$$

where $\gamma_{wan} = 155\pi D^2 k_B^3 / 147\rho v^5 \hbar^4$. If $T_e \gg T_L$, T_e relaxes as a power law³⁵

$$T_e = \frac{T_0}{(1 + 3\gamma_{wan} T_0^3 t)^{1/3}}, \quad (\text{D20})$$

with time scale $1/3\gamma_{wan} T_0^3$ but if $T_e \gtrsim T_L$, T_e relaxes exponentially with time scale $1/\gamma_{wan} T_L^3$

b. High-density limit

Using Eqns. D8, D9 and D16 we have to leading order³⁵

$$\frac{d}{dt} k_B T_e \sim -\gamma_{wad} \frac{1}{T_e} (T_e - T_L), \quad (\text{D21})$$

where $\gamma_{wad} = D^2 \mu^4 / 3\pi^3 \rho v^5 \hbar^4$. So, for $T_e \gg T_L$ the relaxation is linear

$$k_B T_e \sim k_B T_0 - \gamma_{wad} t, \quad (\text{D22})$$

with a rate that goes as $\sim n^{4/3}$ with electron density. In the limit $T_e \gtrsim T_L$, the relaxation is exponential with time scale $T_L / \gamma_{wad} \sim n^{-4/3}$.

Appendix E: Phonon cooling power in graphene

In this section we calculate the temperature relaxation in graphene due to acoustic and optical phonons. The dispersion relation of quasiparticles near a nodal point is $\epsilon_{n\mathbf{k}} = nv\hbar k$ where $k = |\mathbf{k}|$ is a 2D wave vector.

1. Optical phonons

Following the same steps as in Appendix B and using $\omega_{\mathbf{q}} = \omega_0$ and $M_{\mathbf{q}} = g^2/V$ we obtain³⁴

$$\mathcal{P}_{go} = \frac{g^2\omega_0^4}{2\pi v^4\hbar} F(N_e - N_L) \quad (\text{E1})$$

where F is given in Eqn. 9 and Eqns. 13 and 19 are valid for graphene too.

a. Low-density limit

case 1: ($\hbar\omega_0 \gg k_B T_e \gg T_L, \mu$). The energy and particle density $\mathcal{E} = v\hbar I_{2+}/2\pi$ and $n = I_{1-}/2\pi$ are the same as for NLSMs (Eqns. 14 and 15) except for a trivial factor of Q which is absent in graphene. Defining as before $\bar{\beta} \equiv \hbar\omega_0/k_B T_e$ and using E1 we find

$$\frac{\partial \bar{\beta}}{\partial t} = \gamma_{gon1} (\bar{\beta}^4 + 36\zeta(3)\bar{\beta} + \dots) e^{-\bar{\beta}} \quad (\text{E2})$$

where $\gamma_{gon1} = g^2\omega_0/54\zeta(3)v^2\hbar^2$ and to leading order in $\bar{\beta} \gg 1$ we obtain an inverse log form

$$k_B T_e = \frac{\hbar\omega_0}{\log(\gamma_{gon1}\bar{\beta}_0^4 t + e^{\bar{\beta}_0})}, \quad (\text{E3})$$

case 2: ($k_B T_e \gg \hbar\omega_0, k_B T_L, \mu$). In the opposite regime where $k_B T_e \gg \hbar\omega_0$ the same considerations apply as in NLSMs and we obtain an exponential relaxation, see Eqn. 20, but the factor of Q is absent in graphene.

b. High-density limit

The considerations of Sec. III B apply for graphene as well. We obtain the same relaxation forms as in Eqn. 25

and 27 but the factor of Q is absent in graphene.

2. Acoustic phonons

The temperature relaxation due to acoustic phonon scattering in NLSMs and graphene are different because the nodal line affects NLSMs in a nontrivial way, see Appendix C. The temperature relaxation in graphene due to acoustic phonons was presented by Bistrizter and MacDonald³⁴ and is included here for comparison with NLSMs. From Eqn. 6 we obtain

$$\mathcal{P}_{ga} = \frac{D^2 k_B}{\rho v^2 \hbar 2\pi} I_{3+}(T_e - T_L) \quad (\text{E4})$$

where I_{3+} is given in Eqn. C8 and in closed form in Ref. 38.

a. Low-density limit

Eqns. 14 and 15 in the limit $\mu \ll k_B T_e$ are also valid for graphene if we omit the factor of Q . From the equation of motion $(\partial\mathcal{E}/\partial T_e)(\partial T_e/\partial t) = -\mathcal{P}_{ga}$ we obtain

$$\frac{dT_e}{dt} = -\gamma_{gan} T_e^2 (T_e - T_L) \quad (\text{E5})$$

where $\gamma_{gan} = D^2 k_B^2 7\pi^4 / 540\zeta(3)\rho v^4 \hbar^3$. This means $T_e = T_0/(1 + t/\tau_{gan})^{1/2}$ for $T_e \gg T_L$. T_e is an exponential function with time scale $1/\gamma_{gan} T_L^2$ for $T_e \gtrsim T_L$.

b. High-density limit

Eqns. 22 and 23 are also valid for graphene after omitting the factor of Q and we obtain

$$\frac{dT_e}{dt} = -\gamma_{gad} \frac{1}{T_e} (T_e - T_L), \quad (\text{E6})$$

where $\gamma_{gad} = 3D^2 \mu^3 / 4\pi^2 k_B \rho v^4 \hbar^3$. This means the relaxation is linear for $T_e \gg T_L$ and the rate scales as $\sim n^{3/2}$ with electron density. The relaxation is exponential for $T_e \gtrsim T_L$.

¹ V. F. Gantmakher and Y. B. Levinson, *Carrier scattering in metals and semiconductors* (Elsevier Science Publishers, NY, 1987).

² S. M. Sze, Y. Li, and K. K. Ng, *Physics of Semiconductor Devices* (Wiley; 4th edition, 2021).

³ P. B. Allen, Phys. Rev. Lett. **59**, 1460 (1987).

⁴ F. C. Wellstood, C. Urbina, and J. Clarke, Phys. Rev. B **49**, 5942 (1994).

⁵ M. Massicotte, G. Soavi, A. Principi, and K.-J. Tielrooij, Nanoscale **13**, 8376 (2021).

⁶ A. Sergeev and V. Mitin, Phys. Rev. B **61**, 6041 (2000).

⁷ J. T. Karvonen, L. J. Taskinen, and I. J. Maasilta, Phys. Rev. B **72**, 012302 (2005).

- ⁸ F. W. J. Hekking, A. O. Niskanen, and J. P. Pekola, *Phys. Rev. B* **77**, 033401 (2008).
- ⁹ S. S. Kubakaddi, *Phys. Rev. B* **79**, 075417 (2009).
- ¹⁰ N. P. Armitage, E. J. Mele, and A. Vishwanath, *Rev. Mod. Phys.* (2018).
- ¹¹ H. L. Stormer, L. N. Pfeiffer, K. W. Baldwin, and K. W. West, *Phys. Rev. B* **41**, 1278 (1990).
- ¹² D. K. Efetov and P. Kim, *Phys. Rev. Lett.* **105**, 256805 (2010).
- ¹³ W.-K. Tse and S. Das Sarma, *Phys. Rev. B* **79**, 235406 (2009).
- ¹⁴ J. C. W. Song, M. Y. Reizer, and L. S. Levitov, *Phys. Rev. Lett.* **109**, 106602 (2012).
- ¹⁵ J. Coulter, G. B. Osterhoudt, C. A. C. Garcia, Y. Wang, V. M. Plisson, B. Shen, N. Ni, K. S. Burch, and P. Narang, *Phys. Rev. B* **100**, 220301 (2019).
- ¹⁶ G. B. Osterhoudt, Y. Wang, C. A. C. Garcia, V. M. Plisson, J. Gooth, C. Felser, P. Narang, and K. S. Burch, *Phys. Rev. X* **11**, 011017 (2021).
- ¹⁷ A. A. Burkov, M. D. Hook, and L. Balents, *Phys. Rev. B* **84**, 235126 (2011).
- ¹⁸ Y. Kim, B. J. Wieder, C. L. Kane, and A. M. Rappe, *Phys. Rev. Lett.* **115**, 036806 (2015).
- ¹⁹ C. Fang, Y. Chen, H.-Y. Kee, and L. Fu, *Phys. Rev. B* **82**, 081201 (2015).
- ²⁰ C. Fang, H. Weng, X. Dai, and Z. Fang, *Chinese Physics B* **25**, 117106 (2016).
- ²¹ G. Bian, T.-R. Chang, *et al.*, *Nature Communications* **7**, 10556 (2016).
- ²² Y. Wu, L.-L. Wang, E. Mun, D. D. Johnson, D. Mou, L. Huang, Y. Lee, S. L. Bud'ko, P. C. Canfield, and A. Kaminski, *Nature Physics* **12**, 667 (2016).
- ²³ L. M. Schoop, M. N. Ali, C. Straßer, A. Topp, A. Varykhalov, D. Marchenko, V. Duppel, S. S. P. Parkin, B. V. Lotsch, and C. R. Ast, *Nature Communications* **7**, 11696 (2016).
- ²⁴ M. Neupane, I. Belopolski, M. M. Hosen, D. S. Sanchez, R. Sankar, M. Szlowska, S.-Y. Xu, K. Dimitri, N. Dhakal, P. Maldonado, P. M. Oppeneer, D. Kaczorowski, F. Chou, M. Z. Hasan, and T. Durakiewicz, *Phys. Rev. B* **93**, 201104 (2016).
- ²⁵ S.-Y. Yang, H. Yang, E. Derunova, S. S. P. Parkin, B. Yan, and M. N. Ali, *Advances in Physics: X* **3**, 1414631 (2018).
- ²⁶ S. Klemenz, S. Lei, and L. M. Schoop, *Annual Review of Materials Research* **49**, 185 (2019).
- ²⁷ M. N. Ali, L. M. Schoop, C. Garg, J. M. Lippmann, E. Lara, B. Lotsch, and S. S. P. Parkin, *Science Advances* **2**, e1601742 (2016).
- ²⁸ G. Gatti, A. Crepaldi, M. Puppini, N. Tancogne-Dejean, L. Xian, U. De Giovannini, S. Roth, S. Polishchuk, P. Bugnon, A. Magrez, H. Berger, F. Frassetto, L. Polletto, L. Moreschini, S. Moser, A. Bostwick, E. Rotenberg, A. Rubio, M. Chergui, and M. Grioni, *Phys. Rev. Lett.* **125**, 076401 (2020).
- ²⁹ Y. Shao, A. N. Rudenko, J. Hu, Z. Sun, Y. Zhu, S. Moon, A. J. Millis, S. Yuan, A. I. Lichtenstein, D. Smirnov, M. I. K. Z. Q. Mao, and D. N. Basov, *Nat. Phys.* **16**, 636–641 (2020).
- ³⁰ S. T. Ramamurthy and T. L. Hughes, *Phys. Rev. B* **95**, 075138 (2017).
- ³¹ A. N. Rudenko, E. A. Stepanov, A. I. Lichtenstein, and M. I. Katsnelson, *Phys. Rev. Lett.* **120**, 216401 (2018).
- ³² Y. Huh, E.-G. Moon, and Y. B. Kim, *Phys. Rev. B* **93**, 035138 (2016).
- ³³ S. V. Syzranov and B. Skinner, *Phys. Rev. B* **96**, 161105 (2017).
- ³⁴ R. Bistritzer and A. H. MacDonald, *Phys. Rev. Lett.* **102**, 206410 (2009).
- ³⁵ R. Lundgren and G. A. Fiete, *Phys. Rev. B* **92** (2015).
- ³⁶ B. N. Narozhny and I. V. Gornyi, *Frontiers in Physics* **9**, 108 (2021).
- ³⁷ A. Lucas and K. C. Fong, *Journal of Physics: Condensed Matter* **30**, 053001 (2018).
- ³⁸ J. K. Viljas and T. T. Heikkilä, *Phys. Rev. B* **81**, 245404 (2010).
- ³⁹ Y. H. Wang, D. Hsieh, E. J. Sie, H. Steinberg, D. R. Gardner, Y. S. Lee, P. Jarillo-Herrero, and N. Gedik, *Phys. Rev. Lett.* **109**, 127401 (2012).
- ⁴⁰ A. N. Rudenko and S. Yuan, *Phys. Rev. B* **101**, 115127 (2020).